Chirped pulse upconversion for femtosecond mid-infrared spectroscopy at 100 kHz

Mindaugas Jonušas, Quentin Bournet, Adeline Bonvalet, Michele Natile, Florent Guichard, Yoann Zaouter, Patrick Georges, Frédéric Druon, Marc Hanna, Manuel Joffre

Opt. Express **32**, 8020 (2024) https://doi.org/10.1364/OE.515291

Chirped Pulse Upconversion for femtosecond mid-infrared spectroscopy at 100 kHz

Mindaugas Jonušas[1], Quentin Bournet[2,3], Adeline Bonvalet[1], Michele Natile[3], Florent Guichard[3], Yoann Zaouter[3], Patrick Georges[2], Frédéric Druon[2], Marc Hanna[2], and Manuel Joffre[1]

[1] *Laboratoire d'Optique et Biosciences, Ecole Polytechnique, CNRS, INSERM, Institut Polytechnique de Paris, 91120 Palaiseau, France*
[2] *Université Paris-Saclay, Institut d'Optique Graduate School, CNRS, Laboratoire Charles Fabry, 91127 Palaiseau, France*
[3] *Amplitude, 11 Avenue de Canteranne, Cité de la Photonique, 33600 Pessac, France*

Abstract

We demonstrate that chirped pulse up-conversion (CPU), a method routinely used with systems based on 1-kHz Titanium:Sapphire lasers, can be extended to a repetition rate of 100 kHz with an Ytterbium diode-pumped femtosecond amplifier. Individual mid-infrared spectra can thus be measured directly in the near infrared using a fast CMOS linescan camera. After an appropriate Fourier processing, a spectral resolution of 1.1 cm^{-1} is reported, currently limited by our spectrometer. Additionally, we demonstrate the application of CPU to a pump-probe measurement of the vibrational relaxation in carboxy-hemoglobin, and we show that the combination of fast scanning and fast acquisition enables a straightforward removal of pump scattering interference.

1 Introduction

With their high repetition rates, typically 100 kHz or more, femtosecond diode-pumped Yb-based amplifiers are in the process of revolutionizing ultrafast spectroscopy [1–9]. Indeed, it has been shown that such laser sources provide a huge improvement in signal-to-noise ratio (or equivalently reduced acquisition time), thanks not only to the higher repetition rate but also to the associated increase in modulation frequencies and hence reduced $1/f$ noise [4]. Furthermore, such high repetition-rate lasers are ideally suited for studying multi-timescale dynamics by use of multiple probing [3, 8].

However, in order to take full advantage of these features, it is essential to rely on shot-to-shot detection methods that are able to cope with the high repetition rate of the laser. In the visible or near-infrared spectral domain, this has been achieved using fast linear arrays providing thousands of pixels [4, 7, 9, 10]. In contrast, all experiments reported so far in the mid-infrared (MIR) spectral domain, such as time-resolved vibrational [3] or 2DIR spectroscopy [1, 2, 5, 6, 8], rely on Mercury-Cadmium-Telluride (MCT) arrays, with sometimes custom-designed electronics in order to handle the high repetition rate [6]. The use of MCT arrays results in a substantial cost and in a limited number of pixels, typically 128 or less, hence a limited spectral resolution. An alternative method for MIR femtosecond spectroscopy, combining a lower cost and a greater number of pixels, is thus desirable.

Such an alternative method, Chirped Pulse Upconversion (CPU) [11–22], has been widely used with Titanium:Sapphire (Ti:Sa) femtosecond amplifiers running at a lower repetition rate. CPU consists of mixing the MIR field with a chirped field, of duration typically 100 ps and centered at 800 nm, so that the up-converted pulse can be readily detected in the visible using a standard CCD camera [11]. With an appropriate Fourier processing [13, 14], the spectral resolution is then ultimately determined by the inverse of the chirped pulse duration, or more often by the spectral resolution of the spectrometer. Other up-conversion methods have also been demonstrated for MIR detection [23, 24], sometimes even with a CW pump [25–27].

The emerging method known as up-conversion time stretch infrared spectroscopy [27] is of particular interest, as the spectrometer is replaced with a direct measurement in time domain thanks to a huge stretching of the up-converted pulse. However, this approach – reported up to now only for a MIR wavelength around 3.5 μm – requires a very high acquisition bandwidth and has not been demonstrated yet with amplified laser pulses. In contrast, the success of CPU results from the fact that the uncompressed output of any Ti:Sa Chirped Pulse Amplifier [28] provides a stretched pulse of ideal duration and high intensity. In this article, we show that CPU can be extended to 100-kHz laser sources, provided an appropriate chirped pulse is generated and the CCD camera is replaced with a faster 12-bit CMOS linear array. We illustrate the method by measuring in a MIR pump-probe experiment the well-known vibrational relaxation of carboxy-hemoglobin. We also show that the combination of shot-to-shot detection and fast scanning enables a straightforward removal of pump scattering interference.

2 Experimental setup

The experimental setup is shown in Fig. 1. The MIR source, described in detail elsewhere [29], relies on an Yb-doped fiber amplifier operating at 100 kHz. The output beam of the amplifier, centered at 1030 nm, is split in two using a thin film polarizer (TFP1). The reflected part (60 μJ per pulse) is used to generate signal and idler pulses from a BBO-based Optical Parametric Amplifier (OPA), while the transmitted part (140 μJ per pulse) is mixed with the idler output of the OPA (1 μJ per pulse) in order to produce broadband and tunable MIR pulses by type-II Difference Frequency Generation (DFG) in an $LiGaS_2$ (LGS) crystal. The pump intensity at the LGS crystal is estimated to be 100 GW/cm^2, allowing to produce MIR pulses with a center wavelength tunable from 4 to 8 μm. The optical efficiency at 5 μm is about 1.6% (*i.e.* a quantum efficiency of 7.8%), corresponding to MIR pulses of 3.2 μJ, with a pulse-to-pulse stability of 1% RMS. The spectral width is 110 cm^{-1} FWHM, as measured by a Fourier-transform infrared spectrometer.

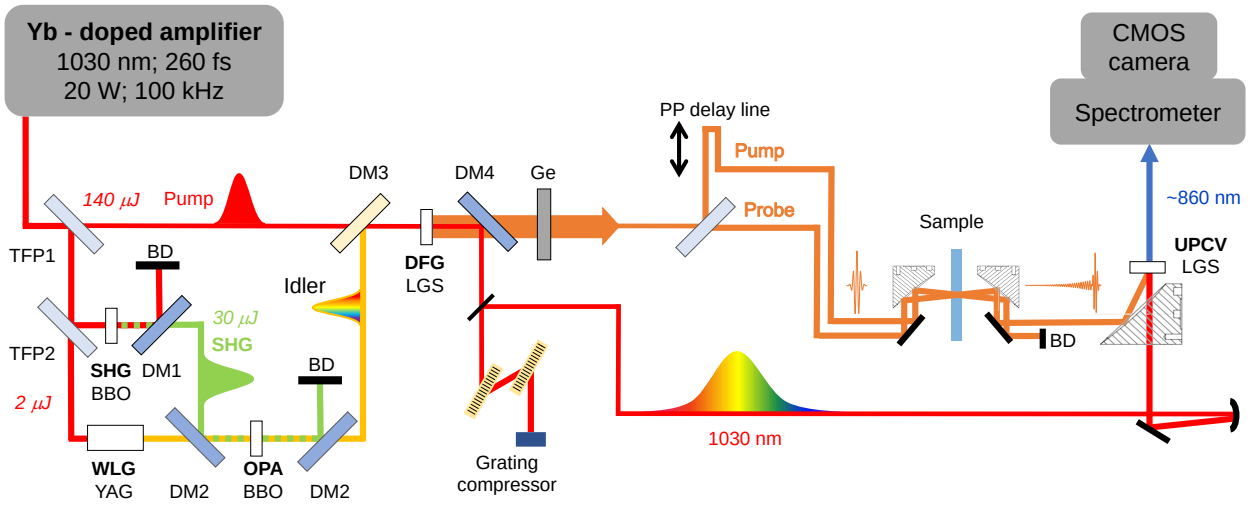

Figure 1: Experimental setup. TFP: thin film polarizer; DM1: dichroic mirror ($R{-}\lambda = 1030$ nm, $T{-}\lambda = 515$ nm); DM2: dichroic mirror ($R{-}\lambda < 1100$ nm, $T{-}\lambda > 1100$ nm); DM3: dichroic mirror ($R{-}\lambda > 1100$ nm, $T{-}\lambda = 1030$ nm); DM4: dichroic mirror ($R{-}\lambda = 1030$ nm, $T{-}$ 4 μm $< \lambda <$ 12 μm); BD: beam dump; Ge: Germanium plate; The two BBO crystals are 2.5-mm thick, the DFG LGS crystal is 2-mm thick, and the up-conversion LGS crystal is 1-mm thick.

Just after the DFG LGS crystal, a ZnSe dichroic mirror (DM4, custom order from Ultrafast Innovations) reflects the remaining 1030-nm pump beam, which is recycled to be later used in the up-conversion process, as shown in Fig. 1. Figure 2 shows the pump spectrum just before and just after the DFG LGS crystal, evidencing a moderate amount of spectral broadening due to self-phase modulation in the LGS crystal. As numerical simulations based on these spectra showed no significant difference on the retrieved MIR spectra in our experimental conditions, we consider that recycling the pump beam is a suitable approach offering the advantage to save valuable photons. An alternative approach would consist of inserting an additional

beam splitter before the OPA in order to extract a 1030-nm beam specifically devoted to CPU, although this method would imply compromising with the available MIR energy or resorting to a more powerful Yb laser.

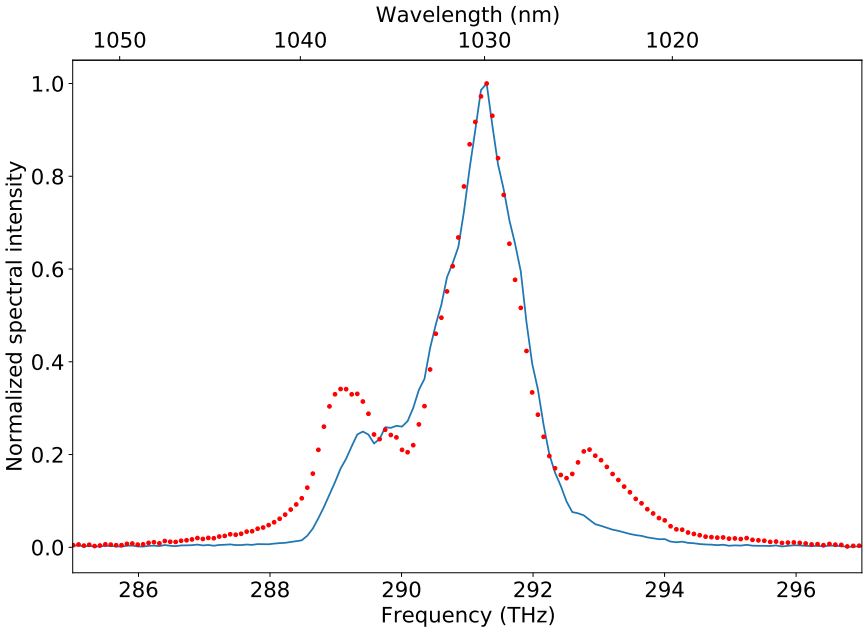

Figure 2: Spectrum of the 1030-nm pump pulse incident on the DFG LGS crystal (blue solid line) and after the DFG LGS crystal (red dots). Both spectra have been normalized to the peak intensity.

Chirped pulses of appropriate duration, typically 50 ps in our experimental conditions, are generated using a grating compressor (1750 grooves/mm transmission gratings, Wasatch Photonics), which acts here as a stretcher delivering negatively-chirped pulses. Spectral resolution and conversion efficiency are both inversely proportional to the chirped pulse duration, so that adjusting the distance between the two gratings is a useful degree of freedom to find the best compromise between these two parameters. Note that stretching the pulse is orders-of-magnitude more energy efficient than the alternative approach of using a narrow-band spectral filter, as keeping the whole spectral bandwidth prevents from throwing away most of the incident pulse energy. Therefore, the additional need for Fourier processing discussed in the next Section is well worth the cost.

The MIR beam transmitted through DM4 and a Germanium plate seeds a pump-probe setup relying on a delay line and a pair of parabolas to focus the beams on the sample. The output probe beam (65 nJ per pulse) is then focused using an off-axis parabolic mirror with through hole (MPD229H-P01, Thorlabs) of reflected focal length 50.8 mm. The chirped beam (50 μJ per pulse) is focused through the hole using a spherical mirror of focal length 200 mm on a 1-mm thick LGS crystal, which has been reported before to be a suitable material for CPU [21]. After reflection on a longpass dichroic mirror (DMLP950, Thorlabs), the up-converted beam is spectrally resolved using a spectrometer (Acton SP-2300i, Princeton Instruments) with a 1200 grooves/mm grating. A fast CMOS camera (Octoplus USB3, Teledyne) allows to record individual spectra up to 120 kHz with a 12-bit resolution. Although 2048 pixels were available, we used only the 1024 pixels in the center of the camera in order to mitigate the effect of vertical astigmatism in the spectrometer.

3 Fourier processing of CPU spectra

We now discuss a first experiment with the pump beam blocked and no sample present in the setup. However, as no dry-air enclosure is used, water molecules are present in the form of water vapor and will be excited along the MIR beam path between the two LGS crystals. Figure 3(a) shows an up-converted spectrum, $S(\omega)$, singled out from a series of probe spectra continuously measured while the laser was running at 100 kHz. The up-converted radiation, resulting from the mixing between the MIR pulse and the 1030-nm chirped pulse, is centered around 860 nm, where it can be readily measured with our CMOS 12-bit camera. The observed spectral width of about 85 cm^{-1}, significantly narrower than the 110-cm^{-1} spectral width of the

incident MIR pulses, is governed by the phase matching bandwidth in our up-conversion LGS crystal. This bandwidth could be extended by using a thinner crystal, at the expense of the conversion efficiency, or by using a different material. Indeed, ultrabroadband capability has been reported as one of the potential advantages of CPU [16].

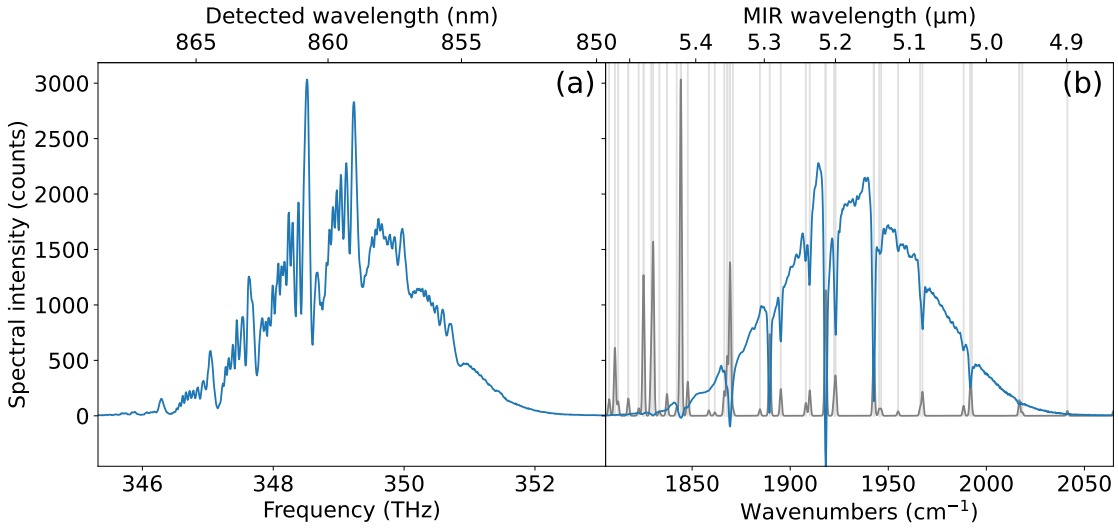

Figure 3: (a) Raw up-converted spectrum, $S(\omega)$, associated with a single laser shot. (b) Corrected spectrum obtained after the Fourier processing discussed in the text (blue line). The gray line shows a water-vapor absorption spectrum computed from the GEISA spectroscopic database [30] and assuming a 1.1-cm^{-1} FWHM.

The strong oscillations observed in Fig. 3(a) result from an effect known as cross phase modulation [13], as the time-domain quadratic phase of the chirped pulse is imprinted onto the up-converted field and yields the observed spectral distortion. Let us summarize the physical origin of this phenomenon, as well as the method routinely used [13, 14] in order to circumvent this effect and retrieve a corrected spectrum such as the one shown in Fig. 3(b). Generally speaking, the MIR field incoming on the up-conversion crystal can be written as $\mathcal{E}(t) = \mathcal{E}_0(t) + \mathcal{E}_R(t)$, where $\mathcal{E}_0(t)$ is the ultrashort MIR field and $\mathcal{E}_R(t)$ is the field radiated by the sample (or here by water molecules) after its excitation by $\mathcal{E}_0(t)$. Due to causality, $\mathcal{E}_R(t)$ extends for positive-only values of time t, covering a timescale of the order of the inverse of the spectral features of the system. After up-conversion, the field can be written as $\mathcal{E}'(t) = \mathcal{E}'_0(t) + \mathcal{E}'_R(t)$, or $\mathcal{E}'(\omega) = \mathcal{E}'_0(\omega) + \mathcal{E}'_R(\omega)$ in frequency domain. The measured spectrum thus reads

$$S(\omega) = |\mathcal{E}'(\omega)|^2 = |\mathcal{E}'_0(\omega)|^2| + \mathcal{E}'^*_0(\omega)\mathcal{E}'_R(\omega) + \mathcal{E}'_0(\omega)\mathcal{E}'^*_R(\omega) + |\mathcal{E}'_R(\omega)|^2. \quad (1)$$

Due to the short duration of the incident MIR pulse with respect to the chirped pulse, it mixes with a well-defined single frequency component of the chirped pulse, corresponding to the frequency ω_0 of the chirped pulse at the time of the overlap between the two pulses. Consequently, $\mathcal{E}'_0(\omega) \propto \mathcal{E}_0(\omega - \omega_0)$ is a mere translated version of the MIR field, with $|\mathcal{E}'_0(\omega)|^2$ being the main contribution to the nearly-gaussian spectrum observed in Fig. 3(a). In contrast, $\mathcal{E}_R(t)$ extends for possibly large time values, so that the mixing will occur with a broad distribution of frequencies from the chirped pulse. For example, the long-lived field associated with a specific rovibrational mode of frequency ω_1 will give rise to an upconverted field $\mathcal{E}'_R(t)$ oscillating not only at frequency $\omega_0 + \omega_1$ but also at smaller frequency values, due to the negative chirp of our linearly-chirped 1030-nm pulse. As the emission delay is proportional to the detuning between $\omega_0 + \omega_1$ and the detected frequency ω, the interference between this field and $\mathcal{E}'_0(\omega)$ (second and third terms in eq. 1) will result in spectral fringes of oscillation period inversely proportional to the detuning. These oscillations will be observed until the period becomes too small to be resolved by the spectrometer. This expected behavior is in perfect agreement with the oscillating features observed for several water lines in Fig. 3(a). We note that, due to the negative value of the chirp, the spectral oscillations are observed on the lower-frequency side of the water lines, in contrast with previous CPU measurements performed with positively-chirped pulses where the oscillations were observed on the higher-frequency side [13].

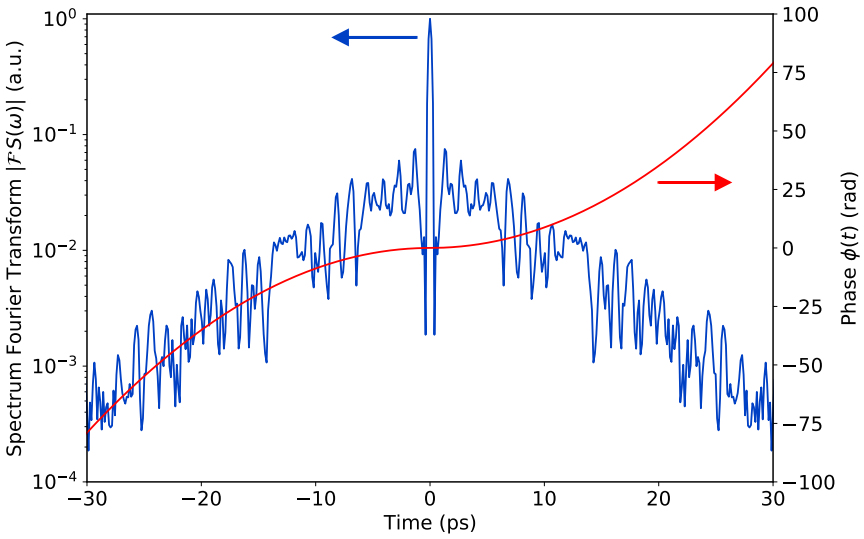

Figure 4: Magnitude of the Fourier transform of the measured spectrum shown in Fig. 3(a), in arbitrary units (blue line). Time-domain phase, $\Phi(t)$, used for correcting the cross-phase modulation associated with the up-conversion process (red line).

As demonstrated previously [13, 14], the effect discussed above can be easily corrected for, provided that we can neglect the last term in eq. 1, $|\mathcal{E}'_R(\omega)|^2$, *i.e.* when the radiated field is small enough with respect to the incident MIR field. Figure 4 shows the quantity $|\mathcal{F}S(\omega)|$, magnitude of the Fourier transform of $S(\omega)$, normalized to its peak value at $t = 0$. Thanks to the above approximation and to the causal nature of the radiated field, the contribution to Fig. 4 of the three remaining terms in eq. 1 can be readily attributed. The narrow central peak is simply the autocorrelation function, $\mathcal{E}_0^*(-t) \otimes \mathcal{E}_0(t)$, of the incident MIR field, *i.e.* the Fourier transform of the first term in eq. 1. The signal obtained for positive times is the correlation function $\mathcal{E}_0^*(-t) \otimes \mathcal{E}_R(t)$, Fourier transform of the second term in eq. 1, while the signal obtained for negative times is the conjugated time-reversed version of its positive-time counterpart (*i.e.* third term in eq. 1). The observed quasi-periodic evolution of the radiated field can be attributed to the quantization of the rotational motion of water molecules, although the asymmetric top rotational structure yields more complicated features. Finally, the roughly exponential decay of the signal can be attributed to the finite resolution of our spectrometer. Correcting for the cross-phase modulation is simply achieved by subtracting to $\mathcal{F}S(\omega)$ the parabolic time-domain phase, $\phi(t) = -t^2/(2\varphi'')\,\mathrm{sign}(t)$, where φ'' is the second-order derivative of the chirped pulse spectral phase [13, 14]. The sign function is required as the data for negative times is not only time reversed but also complex conjugated, hence the need for changing the sign of the phase. An inverse Fourier transform back to frequency domain then yields directly the spectrum shown as a solid blue line in Fig. 3(b), where an excellent spectral resolution is now restored. As the distance between the two gratings is not exactly known, we simply adjusted the value of φ'' in order to optimize the spectral resolution, with an optimal value $\varphi'' = -5.7$ ps^2. We note that no improvement in spectral resolution could be achieved by introducing a third-order phase in $\phi(t)$. This is consistent with the fact that, considering the parameters of our grating compressor, we expect a ratio of -15.8 fs between the third-order and second-order spectral phases, *i.e.* a third-order spectral phase of only 0.09 ps^3 with a negligible effect on the up-converted spectrum. We conclude that the approximation of a purely quadratic spectral phase is appropriate. The retrieved spectrum shown in Fig. 3(b) is in excellent agreement with the absorption spectrum of water vapor, as obtained from the GEISA spectroscopic database [30].

The extremely-narrow water-vapor spectral lines allow to determine the actual spectral resolution of the CPU spectrum after Fourier processing. We thus obtain a spectral resolution of 1.1 cm^{-1} FWHM, which is actually limited by the spectral resolution of our spectrometer. However, it is noteworthy that the approximation consisting of neglecting the last term of eq. 1 (valid when the optical density is much smaller than 1) breaks down for the strongest absorption lines, such as the lines centered on 1918 and 1942.5 cm^{-1}. The resulting imperfect correction generates a sharp peak that can be seen in the transmitted spectrum just below these two spectral lines. The imperfect correction even generates a negative retrieved signal in the

case of the stronger line at 1918 cm^{-1}. However, in practice these strong absorption lines can be removed by using a dry-air enclosure. Furthermore, the approximation mentioned above will always hold when the Fourier processing is directly applied to a small differential signal, which will always be much smaller than the incident MIR signal.

4 Pump-probe experiment

We now discuss a pump-probe experiment that we performed in carboxyhemoglobin (HbCO) using CPU to measure the probe spectral intensity for each probe pulse at the 100-kHz repetition rate of the laser. HbCO was chosen for its well-known properties and widespread use in MIR spectroscopy, but CPU can of course be used for a broad variety of systems. The pump-probe delay is continuously scanned using a translation stage (V-528, Physik Instrumente) driven by a 2-Hz triangular signal. The pump beam is chopped by a mechanical chopper, so that spectra accumulated during each pump-off acquisition period yield an average reference spectrum subtracted to spectra measured during the next pump-on acquisition period. For each pump-on measurement, the corresponding difference spectrum is accumulated in a specific time bin according to the pump-probe delay determined by the voltage provided by the translation stage. The chopping frequency is chosen slightly detuned from 1 kHz (*i.e.* the 500^{th} harmonic of the scanning frequency), so that all time bins are eventually addressed. The HbCO sample has been prepared by dissolving lyophilized powder of human hemoglobin (Sigma) in a tris-HCL buffer. After adding an excess of dithionite the solution is kept under CO atmosphere, and then mounted between two calcium fluoride windows with a 100-μm spacer.

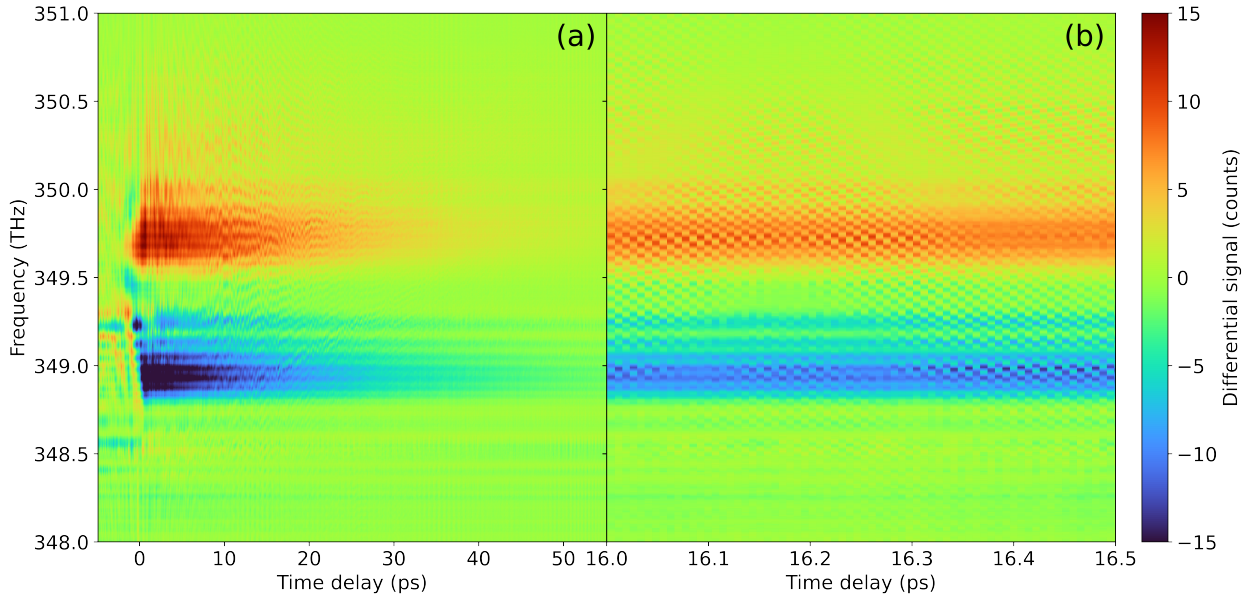

Figure 5: (a) Raw data consisting in a series of 8192 pump-probe spectra. (b) Zoom of the same data around a 500-fs time-delay interval, showing 68 individual spectra and evidencing the fast oscillations (both in frequency and time) due to spectral interference between the probe pulse and pump scattering.

As the sample can be considered to be a parallel-plane plate, no spatial chirp is expected as a result of the sample insertion. However, a well-known issue with CPU is that inserting a sample in the probe beam results in a shift in the measured spectrum, due to the linear time-frequency relation for the chirped pulse. This can be easily dealt with by changing frequency ω_0 in the retrieval program or by translating the chirped-pulse delay line. In both cases, water-vapor absorption lines can be used for an accurate calibration of the up-converted spectrum taking into account the added delay encountered in the sample.

Figure 5(a) shows a series of difference spectra resulting from data averaging over a period of about 5 min. The data are sorted in 8192 different 7.33-fs time bins covering a 60-ps delay range. On top of the expected pump-probe signal, we observe a series of horizontal lines due to the spectral oscillations associated with water-vapor absorption, as discussed in the previous section.Furthermore, for pump-probe delays shorter than 30 ps, we also observe spectral oscillations of varying period that result from the interference between

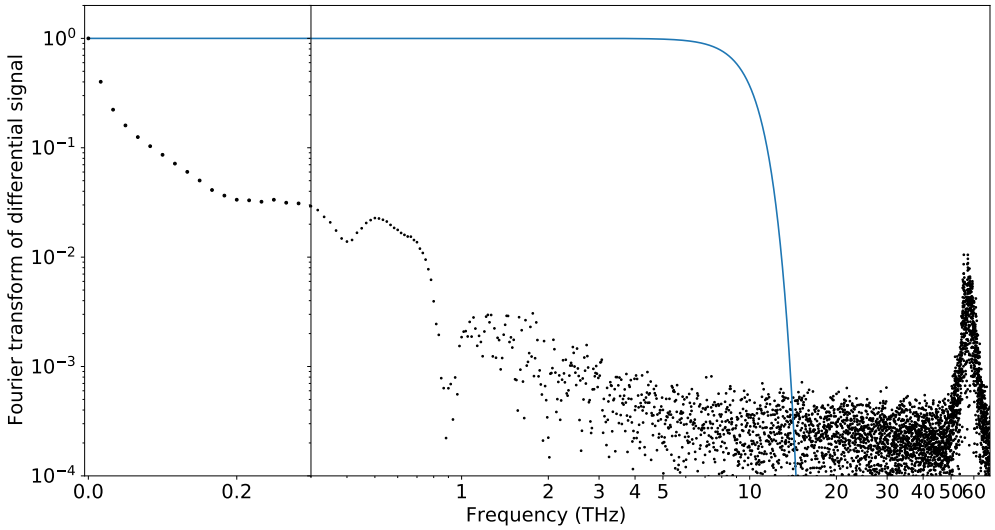

Figure 6: The dots show the magnitude of the inverse Fourier transform with respect to time delay τ of the signal measured at the pixel corresponding to a measured frequency of 348.95 THz, associated with the induced absorption signal. The solid blue line shows the hypergaussian function used to filter out pump scattering. The vertical scale is logarithmic, while the horizontal scale is linear (resp. logarithmic) for frequencies smaller (resp. greater) than 300 GHz.

the probe pulse and scattering from the pump pulse. These spectral fringes are better resolved in Fig. 5(b), which shows a zoomed-in version where the time-delay axis has been expanded to reveal individual time bins. Considering the fact that our 7.33-fs time step is slightly smaller than half the carrier period of the MIR pulse (*i.e.* just on the safe side of the Nyquist limit), the phase shift between two consecutive spectra is close to π, as observed in Fig. 5(b). We used these spectral fringes for an accurate determination, by Fourier-Transform spectral interferometry [31], of the zero delay used in the horizontal axis. However, they must obviously be removed for extracting the actual pump-probe response. This well-known issue of removing pump scattering interference is usually addressed by phase cycling using either a pulse shaper [32, 33] or a piezoelectric actuator [34]. Here, we can take advantage of the fine sampling of the time delay axis in order to remove these spectral oscillations by Fourier filtering in the frequency space conjugate to the time delay axis. Figure 6 shows the magnitude of the inverse Fourier transform with respect to time delay of the signal measured for a single pixel of our camera, corresponding to the center of the excited-state absorption line. The term associated with pump scattering appears as a broad line slightly below 60 THz (*i.e.* 2000 cm^{-1}). Although there is a significant broadening due to the fact that the delay is not known with an interferometric accuracy, this peak is well separated from the actual pump-probe signal which appears at much lower frequencies. Pump scattering can thus be efficiently removed by using an appropriate filter in Fourier space, here an hypergaussian of sixth order with a 10-THz cut-off frequency (solid blue line in Fig. 4).

The whole 2D dataset shown in Fig. 5(a) is thus inverse Fourier transformed with respect to the time delay axis, multiplied by the hypergaussian function to remove pump scattering, and then Fourier transformed back to time domain. The data is then Fourier processed with respect to the probe frequency axis, as described in the previous section, to correct for cross phase modulation associated with CPU. The resulting data is finally divided by the average probe spectrum, where water lines have been Fourier-filtered out. We thus obtain the differential absorption pump-probe data shown in Fig. 7. Apart from a few narrow horizontal lines due to the remaining effect of water vapor absorption, we obtain a clean 2D pump-probe spectrum of the well-known HbCO vibrational response [35], with a bleaching and stimulated emission peak (in blue) corresponding to the 0-1 transition and an excited state absorption peak (in red) corresponding to the 1-2 transition, downshifted by 25 cm^{-1} due to anharmonicity. The spectral oscillations characteristic of perturbed free induction decay can also be observed for negative time delays [36, 37].

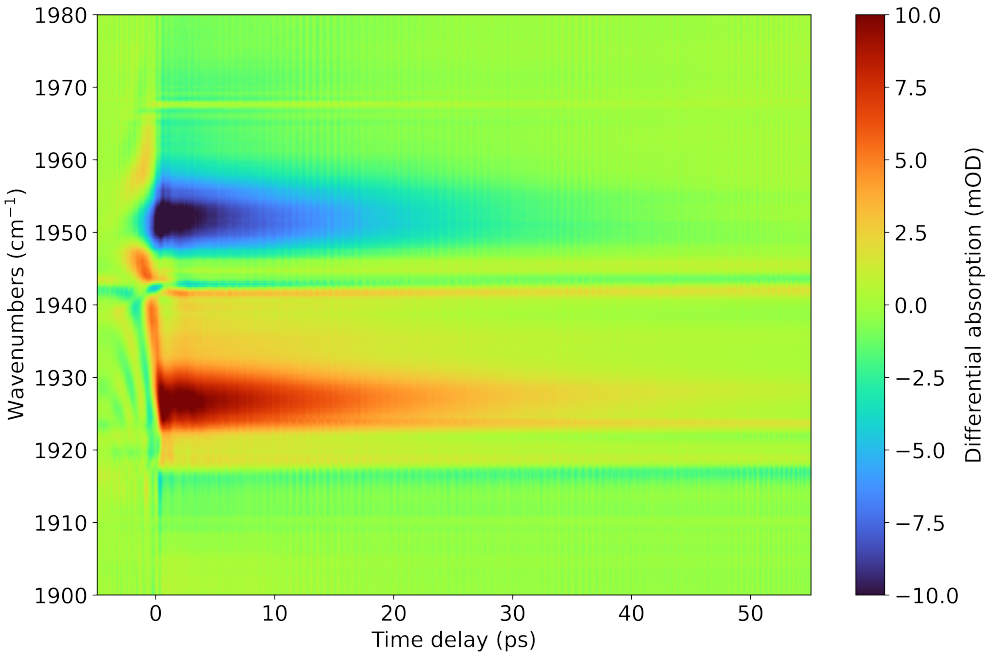

Figure 7: Pump-probe signal obtained after successive Fourier-processings, first with respect to time delay in order to remove pump scattering and, second with respect to the probe frequency to remove the effect of cross phase modulation, as explained in the text.

5 Conclusion

To summarize, we have demonstrated that Chirped Pulse Up-conversion, a method previously used with Ti:Sa 1-kHz laser systems, can be readily used with an Ytterbium diode pumped system running at a repetition rate of 100 kHz. The laser shots can be measured individually using a fast CMOS linescan camera. Using the narrow absorption lines of water vapor in the MIR spectral region, we have demonstrated that a spectral resolution of 1.1 cm^{-1} can be achieved, provided the data are Fourier processed to remove the detrimental effect of cross phase modulation. Both the spectral resolution and the number of usable pixels are currently limited by our spectrometer, but a spectral resolution of 0.5 cm^{-1} combined with the capability of using all 2048 pixels of the camera should be achievable with a higher performance imaging spectrometer free of astigmatism. The acquisition rate of the CMOS camera we used is limited to 120 kHz due to the maximum bit rate of the USB3 bus, but other devices based on a Camera Link connection can run at 250 kHz, which is to our knowledge the fastest rate available for such cameras. In case of lasers with a higher repetition rate, it might eventually be more appropriate to switch to a direct measurement in time domain [27].

Additionally, we have demonstrated the use of CPU in a pump-probe measurement performed in carboxyhemoglobin. The combination of fast scanning and acquisition of individual laser shots enabled an easy removal of the spectral oscillations associated with the interference between the scattered pump and the incident probe, so that we could easily obtain the expected 2D pump-probe spectrum. Using a similar fast-scanning delay line in a Mach-Zehnder interferometer associated with the simultaneous recording of a reference tracer beam should allow to develop a 2DIR spectrometer with a high spectral resolution in both pump and probe dimensions.

Funding Agence Nationale de la Recherche (ANR-19-CE30-0001-MIRTHYX, ANR-10-LABX-0039-PALM).
Disclosures The authors declare no conflicts of interest.
Data availability Data underlying the results presented in this article are available at Zenodo [38].

References

[1] B. M. Luther, K. M. Tracy, M. Gerrity, S. Brown, and A. T. Krummel, Opt. Express **24**, 4117 (2016).

[2] K. M. Tracy, M. V. Barich, C. L. Carver, B. M. Luther, and A. T. Krummel, Journal of Physical Chemistry Letters **7**, 4865 (2016).

[3] G. M. Greetham, P. M. Donaldson, C. Nation, I. V. Sazanovich, I. P. Clark, D. J. Shaw, A. W. Parker, and M. Towrie, Appl. Spectrosc. **70**, 645 (2016).

[4] N. M. Kearns, R. D. Mehlenbacher, A. C. Jones, and M. T. Zanni, Opt. Express **25**, 7869 (2017).

[5] P. M. Donaldson, G. M. Greetham, D. J. Shaw, A. W. Parker, and M. Towrie, J. Phys. Chem. A **122**, 780 (2018).

[6] K. M. Farrell, J. S. Ostrander, A. C. Jones, B. R. Yakami, S. S. Dicke, C. T. Middleton, P. Hamm, and M. T. Zanni, Opt. Express **28**, 33584 (2020).

[7] A. Montanaro, F. Giusti, M. Colja, G. Brajnik, A. M. A. Marciniak, R. Sergo, D. De Angelis, F. Glerean, G. Sparapassi, G. Jarc, S. Carrato, G. Cautero, and D. Fausti, Review of Scientific Instruments **91**, 073106 (2020), https://doi.org/10.1063/5.0016362 .

[8] P. Hamm, J. Chem. Phys. **154**, 104201 (2021).

[9] S. J. Hall, P. J. Budden, A. Zats, and M. Y. Sfeir, Rev. Sci. Instr. **94**, 043005 (2023).

[10] F. Kanal, S. Keiber, R. Eck, and T. Brixner, Opt. Express **22**, 16965 (2014).

[11] K. J. Kubarych, M. Joffre, A. Moore, N. Belabas, and D. Jonas, Opt. Lett. **30**, 1228 (2005).

[12] M. J. Nee, R. McCanne, K. J. Kubarych, and M. Joffre, Opt. Lett. **32**, 713 (2007).

[13] K. F. Lee, P. Nuernberger, A. Bonvalet, and M. Joffre, Opt. Express **17**, 18738 (2009).

[14] J. M. Anna, M. J. Nee, C. R. Baiz, R. McCanne, and K. J. Kubarych, J. Opt. Soc. Am. B **27**, 382 (2010).

[15] P. Nuernberger, K. F. Lee, A. Bonvalet, M. H. Vos, and M. Joffre, J. Phys. Chem. Lett. **1**, 2077 (2010).

[16] C. R. Baiz and K. J. Kubarych, Opt. Lett. **36**, 187 (2011).

[17] J. Zhu, T. Mathes, A. D. Stahl, J. T. M. Kennis, and M. L. Groot, Opt. Express **20**, 10562 (2012).

[18] Y. Nomura, Y. T. Wang, T. Kozai, H. Shirai, A. Yabushita, C. W. Luo, S. Nakanishi, and T. Fuji, Opt. Express **21**, 18249 (2013).

[19] J. Knorr, P. Rudolf, and P. Nuernberger, Opt. Express **21**, 30693 (2013).

[20] W. Rock, Y.-L. Li, P. Pagano, and C. M. Cheatum, J. Phys. Chem. A **117**, 6073 (2013).

[21] R. Nakamura, Y. Inagaki, H. Hata, N. Hamada, N. Umemura, and T. Kamimura, Appl. Opt. **55**, 9365 (2016).

[22] Y. Zhao, S. Kusama, Y. Furutani, W.-H. Huang, C.-W. Luo, and T. Fuji, Nat. Comm. **14** (2023), 10.1038/s41467-023-39628-6.

[23] T. P. Dougherty and E. J. Heilweil, Opt. Lett. **19**, 129 (1994).

[24] M. E. DeCamp and A. Tokmakoff, Opt. Lett. **30**, 1818 (2005).

[25] S. Wolf, J. Kiessling, M. Kunz, G. Popko, K. Buse, and F. Kuehnemann, Opt. Express **25**, 14504 (2017).

[26] N. M. Israelsen, P. J. Rodrigo, C. R. Petersen, G. Woyessa, R. E. Hansen, P. Tidemand-Lichtenberg, C. Pedersen, and O. Bang, Opt. Express **46**, 4558 (2021).

[27] K. Hashimoto, T. Nakamura, T. Kageyama, V. R. Badarla, H. Shimada, R. Horisaki, and T. Ideguchi, Light Sc. Appl. **12**, 48 (2023).

[28] D. Strickland and G. Mourou, Opt. Comm. **56**, 219 (1985).

[29] Q. Bournet, M. Natile, M. Jonusas, F. Guichard, Y. Zaouter, M. Joffre, A. Bonvalet, F. Druon, M. Hanna, and P. Georges, Opt. Express **31**, 12693 (2023).

[30] "GEISA - Spectroscopic database," [retrieved 13 September 2023], `https://geisa.aeris-data.fr/interactive-access/`.

[31] L. Lepetit, G. Cheriaux, and M. Joffre, J. Opt. Soc. Am. B **12**, 2467 (1995).

[32] S. H. Shim, D. B. Strasfeld, Y. L. Ling, and M. T. Zanni, Proc. Natl. Acad. Sci. USA **104**, 14197 (2007).

[33] J. A. Myers, K. L. M. Lewis, P. F. Tekavec, and J. P. Ogilvie, Opt. Express **16**, 17420 (2008).

[34] R. Bloem, S. Garrett-Roe, H. Strzalka, P. Hamm, and P. Donaldson, Opt. Express **18**, 27067 (2010).

[35] J. C. Owrutsky, M. Li, B. Locke, and R. M. Hochstrasser, J. Phys. Chem. **99**, 4842 (1995).

[36] M. Joffre, D. Hulin, A. Migus, A. Antonetti, C. Benoit à la Guillaume, N. Peyghambarian, M. Lindberg, and S. W. Koch, Opt. Lett. **13**, 276 (1988).

[37] P. Hamm, Chem. Phys. **200**, 415 (1995).

[38] "Chirped pulse upconversion for femtosecond mid-infrared spectroscopy at 100 kHz," [retrieved 18 January 2024], `https://zenodo.org/doi/10.5281/zenodo.10528467`.